Local evidence is key to assessing biodiversity vulnerability to climate change

Muyang Lu (muyang.lu@yale.edu)
University College London https://orcid.org/0000-0002-4949-8837
Walter Jetz
Yale University https://orcid.org/0000-0002-1971-7277

Biological Sciences - Article

Keywords: species distribution models, niche, climate change, hypervolume, spatial scaling

Posted Date: December 6th, 2023

DOI: https://doi.org/10.21203/rs.3.rs-3592626/v1

Additional Declarations: There is **NO** Competing Interest.

Title: Local evidence is key to assessing biodiversity vulnerability to climate change

Muyang Lu[1,2*], Walter Jetz[1,2]

[1]Ecology and Evolutionary Biology, Yale University, New Haven, CT, 06511, USA

[2]Center for Biodiversity and Global Change, Yale University, New Haven, CT, 06511, USA

*Present address: Centre for Biodiversity and Environment Research, Department of Genetics, Evolution and Environment, University College London, London, UK.

Corresponding author:

Muyang Lu (muyang@gmail.com) and Walter Jetz (walter.jetz@yale.edu)

Words in the abstract: 182

Words in the main text: 2263

Number of display items: 4 figures

Key words: species distribution models; niche; climate change; hypervolume; spatial scaling

Abstract

Gaging the effects of impending climate change on biodiversity is one of the most pressing scientific challenges[1,2]. Recent studies have indicated the risk of widespread range contraction[3] and community collapse[4] globally, but their specific interpretation and decision-relevance is constrained by the coarse-grain nature of their underlying evidence[5]. Here, we demonstrate for 1,804 Western Hemisphere bird species that coarse-grain estimates of climate change vulnerability show limited correspondence with those derived from biologically more appropriate local data. Coarse-grain data used widely in recent assessments miss up to half of the most vulnerable species due to significant errors of omission and commission that covary with spatial autocorrelation and ecological attributes of species. This strongly affects the perceived vulnerability of high-biodiversity tropical regions– , for example, species in the Amazon region are even more vulnerable to climate change than previously reported[4]. These findings alter the insights of recent global work and highlight the importance of considering the scale of available evidence[7,8]. Informed collection of local data combined with model-based data fusion[9,10] will be key for effectively assessing and managing the effects of climate change on biodiversity.

Ongoing and future climate change poses an immense threat to biodiversity[4,11,12], and assessing how and where climatic change is affecting individual species globally is central to supporting effective conversation and management[13–15]. Ample evidence points to an accelerating perturbation and erosion of the tightly evolved environmental associations, or niches, of species and resulting losses of populations and geographic distributions[16,17]. Robust avenues for identifying species and regions particularly vulnerable to climate change are thus key. For select species and specific locations, eco-physiological and activity data have been able to support mechanistically informed, fine-tuned projections[18,19]. But more comprehensive assessments tend to rely on large-extent, coarse-grain species distribution evidence to evaluate species climatic niches and future risks[3,4,20,21]. The widespread exposure to extreme climates[3,21] and sudden collapses of global biodiversity[3,4] reported by these efforts have garnered notable attention. Their specific insights include that species in regions with limited climatic heterogeneity such as the Amazon basin face greater risks than those in mountains[6] . A key unaddressed aspect, however, is how much the coarse-grain analysis accurately reflects a species' association with its living habitat and environment[5,10,22].

The dependence of environmental niche characterizations on spatial grain has long been recognized[8,23,24], and there is growing appreciation that the strength and form of this link in turn varies with ecological factors[7,25,26]. In most work to date, the resolution of readily available environmental data has driven the spatial grain of analysis rather than the true spatial accuracy of biodiversity data or biological understanding[7]. Critically, however, in the context of climate change, a mismatch between the scale of relevant biological processes and that of evidence has the potential to cause biased vulnerability estimates and erroneous conservation insights[5,23]: exposure and vulnerability studies conducted at coarse spatial grain might only insufficiently and inconsistently capture the finer-grain mechanisms of

vulnerability and deliver results that are disconnected from the processes experienced by the organisms[5,27,28].

While several empirical studies show that coarse-grain data tend to overestimate species' sensitivity to climate change[28–30], theory suggests that the opposite is equally likely[7]. For example, coarse-grain data could underestimate species' sensitivity to climate change by overestimating its climatic tolerance for species with highly specialized habitats within a landscape[7]. To date, the lack of a large scale evaluation has put in question both the magnitude and specificity of biodiversity risk of climate change asserted by recent work[5]. Here we address this issue by assessing the grain-size dependence of vulnerability estimates for a comprehensive system, birds of the Western Hemisphere. The region's avifauna includes many already threatened species with large purported differences in climate change vulnerability and corresponding conservation recommendations[31]. Specifically, we test whether the coarse spatial grains typical for continental to global-scale assessments are able to represent vulnerability experienced at biologically relevant finer (local) grains and how a potential discrepancy covaries with attributes of species and landscapes. To evaluate the relative importance of different climatic niche axes and their interactions with scale and assessed vulnerability, we use a novel partitioning framework based on Hutchinson's n-dimensional hypervolume[32].

Coarse-grain evidence insufficiently captures local vulnerability

Three example species illustrate the strongly different effects scale has on projected climate change vulnerability (Fig. 1). Conditions across the Berylline hummingbird's range in the arid landscapes of central America are projected to be significantly warmer and drier in ca. 30 years compared to today when characterized with local data (1km grain size). But relative to the species niche breadth' at the same resolution (graphically represented as ellipse Fig.

84 1B) this change appears moderate: the species vulnerability score is small (for calculation see
85 inset of Fig. 1B and Fig. 3A), ca 0.5 (Fig. 3C), implying a drop of ca. 20% in future
86 suitability at the niche center. This vulnerability varies little with scale and is similar for
87 coarse-grain data (128km) of the sort used for large-scale analyses[4]. This is different for the
88 White-eared jacamar which, when analyzed with local data, faces a climatic exposure that is
89 substantial in relation to its narrow niche-breadth. Its local-data vulnerability score of 19 puts
90 it into the top 0.1% of Western hemisphere birds most threatened by climate change (Fig.
91 2A). This understanding of climate risk, however, is progressively less appreciated with less
92 fine grains: for coarse-grain data its estimated vulnerability is up to 20 times lower putting
93 the jacamar into the least affected third of species. This scale-dependence arises almost
94 exclusively due to changes in niche breadth, with exposure itself showing relatively low
95 scale-dependence (Fig. 1B). The Brazilian ruby shows the opposite pattern. Here the coarse-
96 grain assessment suggests a large vulnerability of ca. 4, i.e. among the top 25% of impacted
97 species (Fig. 2B). But analysis with ecologically more relevant local data delivers a greater
98 estimated niche breadth suggests this to be a 'false positive' (Fig. 1B, compare size of
99 ellipses). The species exhibits a positive vulnerability - grain relationship, with a change to
100 just 0.8 vulnerability and thus roughly in the bottom half of all species analyzed with local
101 data.
102
103 Across all 1,804 assessed species, only about half of 20% assessed as most vulnerable by
104 either coarse-grain and local data are shared between those two grains (Fig. 2). Overall,
105 climate change vulnerability shows a highly heterogeneous scaling pattern that is very strong
106 for some species (Fig. 3C). And among the two orders of magnitude of grain sizes assessed
107 vulnerabilities are highly discrepant, with a Pearson correlation of just 0.43 between coarse-
108 grain and local values (Fig. 3D, Extended Data Fig. 1). 30% of the 1804 species differ by

more than 0.45 in vulnerability between coarse-grain and local values (an increase of 0.45 vulnerability score corresponds to a 20% drop in suitability at the niche center); for ca. 15% of the species this vulnerability difference is more than 1 (corresponding to a 40% drop), and for 8% of the species the vulnerability change is more than 2 (corresponding to a 70% drop). Partitioned into the core components, we find that temperature is the key driver of climate change vulnerability for our three example species (Fig. 3B, Extended Data Fig. 2-3). This pattern generally extends to all assessed species, for which temperature vulnerability contributes most strongly to vulnerability and to the observed scale dependence (Fig. 3C, D).

Biological and landscape factors drive the spatial scaling of vulnerability

We find that a range of biological and landscape factors explain these scaling differences among species (Fig. 4A). Temperature and precipitation auto-correlation across the landscapes a species occurs in has by far the greatest effect (Fig. 4A). In landscapes where nearby places have similar temperatures (e.g., places with low terrain variation), it is very likely that an analysis with coarse-grain data misses species with high vulnerability. The opposite is true for precipitation: species in areas of strong geographic precipitation variability tend to be less vulnerable than coarse-grain data might suggest. Other geographic and biological species attributes play a weaker role (Fig. 4A). These results are robust across climate change models, scenarios, and spatial thinning distances (Extended Data Fig. 4-9).

Tropical regions are more vulnerable when assessed with local data

The strong role of landscape factors suggests that the scale dependence of vulnerability varies geographically. Mapping the mean local vs. coarse-grain vulnerability of assessed species we find the tropics to be much more sensitive to grain size than temperate areas (Fig. 4B). Specifically, the climate change vulnerability of species in the Amazon basin, the Atlantic

Forest, and the Caribbean islands are more likely to be impacted by the choice of grain size than species in other regions. There, up to 40% of species might have an absolute change of vulnerability greater than 0.45 between local and coarse grains (Extended Data Fig. 10). Accordingly, the hotspots of most vulnerable species differ substantially across grains (Fig. 4B), with species in the Atlantic Forest emerging as less and those in the Amazonian basin as more vulnerable species when assessed with local compared to coarse-grain data.

Despite the central importance of spatial scale in ecology and conservation[24,33] and a growing recognition of the issue[34,35], how spatial scale affects the assessment of species climate change vulnerability has seen limited study [5,28,36]. We find that a significant portion of species show great scale dependence in their vulnerability. These highly scale-sensitive species drive a very low congruence between the most vulnerable species identified with coarse-grain vs. local data. At minimum, this suggests that estimates of species climate change exposure and vulnerability are much less reliable than analyses conducted at a single grain might suggest. But given that for almost all the assessed species home range sizes and mechanistic response grains[25] are not expected to exceed 1km, this observed mismatch has additional, more concrete implications[5,35,37]. Coarse-grain data work might have missed important high-exposure and -vulnerability species and places and might have falsely drawn attention to species and areas that might in fact not be as strongly affected. Specifically, we find that assemblages at the Eastern slope of the Andes and in the Amazon basin might be even more vulnerable to climate change than recent studies suggested[4,6], and some more coastal land locations (e.g., the Atlantic forests) potentially less impacted.

Discussion

158 The finding that landscape factors such as environmental autocorrelation have a dominant
159 effect highlights the major role of geographic contingency in robustly estimating climate
160 change vulnerability. Depending on the nature of the variable considered, species in both
161 heterogeneous and homogeneous landscapes can have highly scale-variant climate change
162 vulnerabilities, and so do species that are narrow-ranged and habitat specialist. Such species
163 are more likely to be found in the tropics than in the temperate zones. The Amazon basin
164 emerging as one of the most scale-sensitive region might appear counter-intuitive given its
165 seemingly relatively homogenous temperature and precipitation regime [6]. This phenomenon
166 arises from this region's high temperature auto-correlation inflating coarse-grain niche
167 breadth estimates (Fig. 3B). It means the suggested abrupt impacts of climate change in this
168 region[4,6] might yet be underestimated[5].
169
170 In the presented joint consideration, temperature vulnerability emerges as the major driving
171 force of the multivariate vulnerability compared to precipitation vulnerability and the
172 interaction component. This result supports the general notion of threats from warming on
173 animals' performance and thermal niches as particularly concerning[4,38]. However, our
174 findings do not discount the relevance of precipitation change, because precipitation still
175 affects species indirectly e.g. through changes in vegetation structure and food sources[39].
176 Our study is subject to various limitations common to large-scale studies which, however, we
177 expect to contribute to an underestimation of the issue of scale-sensitivity. For example, our
178 analysis is restricted to species with sufficient occurrence data, but under-sampled species are
179 more likely to be rare, specialized, located in biodiversity hotspots[40,41] and therefore likely
180 scale-sensitive. This suggests that our results might yet underestimate the importance of
181 scale. Further, as data availability limited us to 1km as local data grain, extending the
182 assessment to yet finer grains and their microclimates will likely flag even greater cross-grain

183 inconsistencies and modulate some of the specific results[28,42]. Broadly, however, the results
184 presented here firmly illustrate how the recent generation of near-global coarse-grain findings
185 will need to be updated with work that addresses the uncovered biases from scale-variant
186 vulnerabilities. We suggest that doing so will require a combination of scale-conscious
187 additional sampling, model-supported fusion of different data types, mechanism-informed
188 identifications of optimal analysis grains[43], or multi-scale analytical approaches[25].
189
190 Evidently less limited by gaps and biases of incidental point records or the complexities of
191 species distribution models based on them[10,41], expert range maps or basic among-points
192 interpolation methods offer a strong avenue to address the geographic distribution of speciose
193 taxa globally[44]. But their typically high and ecologically non-random false presence rates
194 when analyzed at resolutions < 100-150km means the scale issues we demonstrated here are
195 necessarily incurred[22]. Even as some recent global studies might have chosen a 25-50km
196 grains for analysis, this does not alter the coarse-grain nature of the signal underpinning
197 expert map data provides[22]. In this case, inferring environmental niches at a finer grain than
198 the expert maps allow more false presences which could seriously underestimate the climate
199 change sensitivity of specialized species in highly heterogeneous landscapes. And we find
200 that smaller, e.g. factor 30-50 grain size differences, still can have vast effects on estimated
201 vulnerabilities (Fig 2, S1), implying that even when captured accurately, occupancy at 25-
202 50km grain might not recover true fine grain sensitivity.
203
204 This highlights the importance of additional collection of local data[9,41]. Assessments like ours
205 might be able to help in prioritizing the species, regions, and locations in greatest need of
206 fine-scale climate change-relevant evidence. Alongside, fusion of different biodiversity data
207 types and models can assist in overcoming their accuracy-coverage trade-offs[10,30] and in

gaging the potential effect of scale variance[10]. A combination of informed field data collection and robust quantitative tools will be key to effectively safeguard biodiversity in a rapidly changing world.

References

1. Bellard, C., Bertelsmeier, C., Leadley, P., Thuiller, W. & Courchamp, F. Impacts of climate change on the future of biodiversity. *Ecol. Lett.* **15**, 365–377 (2012).
2. Araújo, M. B. & Rahbek, C. How does climate change affect biodiversity? *Science.* **313**, 1396–1397 (2006).
3. Pigot, A. L., Merow, C., Wilson, A. & Trisos, C. H. Abrupt expansion of climate change risks for species globally. *Nat. Ecol. Evol.* **7**, 1060–1071 (2023).
4. Trisos, C. H., Merow, C. & Pigot, A. L. The projected timing of abrupt ecological disruption from climate change. *Nature* **580**, 496–501 (2020).
5. Colwell, R. K. Spatial scale and the synchrony of ecological disruption. *Nature* **599**, E8–E10 (2021).
6. Trisos, C. H., Merow, C. & Pigot, A. L. Reply to: Spatial scale and the synchrony of ecological disruption. *Nature* **599**, E11–E13 (2021).
7. Lu, M. & Jetz, W. Scale-sensitivity in the measurement and interpretation of environmental niches. *Trends Ecol. Evol.* **38**, 554–567 (2023).
8. Nadeau, C. P., Urban, M. C. & Bridle, J. R. Coarse climate change projections for species living in a fine-scaled world. *Glob. Chang. Biol.* **23**, 12–24 (2017).
9. Gonzalez, A. *et al.* A global biodiversity observing system to unite monitoring and guide action. *Nat. Ecol. Evol.* (2023). doi:10.1038/s41559-023-02171-0
10. Jetz, W. *et al.* Essential biodiversity variables for mapping and monitoring species

populations. *Nat. Ecol. Evol.* **3**, 539–551 (2019).

11. Barnosky, A. D. *et al.* Has the Earth's sixth mass extinction already arrived? *Nature* **471**, 51–57 (2011).

12. Urban, M. C. Accelerating extinction risk from climate change. *Science.* **348**, 571–573 (2015).

13. Díaz, S. *et al.* The IPBES Conceptual Framework — connecting nature and people. *Curr. Opin. Environ. Sustain.* **14**, 1–16 (2015).

14. Hoffmann, S. & Beierkuhnlein, C. Climate change exposure and vulnerability of the global protected area estate from an international perspective. *Divers. Distrib.* **26**, 1496–1509 (2020).

15. Trew, B. T. & Maclean, I. M. D. Vulnerability of global biodiversity hotspots to climate change. *Glob. Ecol. Biogeogr.* **30**, 768–783 (2021).

16. Antão, L. H. *et al.* Climate change reshuffles northern species within their niches. *Nat. Clim. Chang.* **12**, 587–592 (2022).

17. Viana, D. S. & Chase, J. M. Increasing climatic decoupling of bird abundances and distributions. *Nat. Ecol. Evol.* **6**, 1299–1306 (2022).

18. Riddell, E. A. *et al.* Exposure to climate change drives stability or collapse of desert mammal and bird communities. *Science.* **371**, 633–636 (2021).

19. Kearney, M. & Porter, W. P. Mapping the fundamental niche: Physiology, climate, and the distribution of a nocturnal lizard. *Ecology* **85**, 3119–3131 (2004).

20. Pinsky, M. L., Eikeset, A. M., McCauley, D. J., Payne, J. L. & Sunday, J. M. Greater vulnerability to warming of marine versus terrestrial ectotherms. *Nature* **569**, 108–111 (2019).

21. Murali, G., Iwamura, T., Meiri, S. & Roll, U. Future temperature extremes threaten land vertebrates. *Nature* **615**, 461–467 (2023).

22. Hurlbert, A. H. & Jetz, W. Species richness, hotspots, and the scale dependence of range maps in ecology and conservation. *Proc. Natl. Acad. Sci.* **104**, 13384–13389 (2007).

23. Guisan, A., Graham, C. H., Elith, J. & Huettmann, F. Sensitivity of predictive species distribution models to change in grain size. *Divers. Distrib.* **13**, 332–340 (2007).

24. Wiens, J. A. Spatial scaling in ecology. *Funct. Ecol.* **3**, 385–397 (1989).

25. Mertes, K. & Jetz, W. Disentangling scale dependencies in species environmental niches and distributions. *Ecography.* **41**, 1604–1615 (2018).

26. Connor, T. *et al.* Effects of grain size and niche breadth on species distribution modeling. *Ecography.* **41**, 1270–1282 (2018).

27. Scheffers, B. R., Edwards, D. P., Diesmos, A., Williams, S. E. & Evans, T. A. Microhabitats reduce animal's exposure to climate extremes. *Glob. Chang. Biol.* **20**, 495–503 (2014).

28. Maclean, I. M. D. & Early, R. Macroclimate data overestimate range shifts of plants in response to climate change. *Nat. Clim. Chang.* **13**, 484–490 (2023).

29. Nadeau, C. P., Giacomazzo, A. & Urban, M. C. Cool microrefugia accumulate and conserve biodiversity under climate change. *Glob. Chang. Biol.* **28**, 3222–3235 (2022).

30. Meineri, E. & Hylander, K. Fine-grain, large-domain climate models based on climate station and comprehensive topographic information improve microrefugia detection. *Ecography.* **40**, 1003–1013 (2017).

31. Bateman, B. L. *et al.* North American birds require mitigation and adaptation to reduce vulnerability to climate change. *Conserv. Sci. Pract.* **2**, (2020).

32. Hutchinson, G. E. Concluding remarks. *Cold Spring Harb. Symp. Quant. Biol.* **22**, 415–427 (1957).

33. Levin, S. A. The problem of pattern and scale in ecology. *Ecology* **73**, 1943–1967

(1992).

34. Zellweger, F., De Frenne, P., Lenoir, J., Rocchini, D. & Coomes, D. Advances in microclimate ecology arising from remote sensing. *Trends Ecol. Evol.* **34**, 327–341 (2019).

35. Lembrechts, J. J., Nijs, I. & Lenoir, J. Incorporating microclimate into species distribution models. *Ecography.* **42**, 1267–1279 (2019).

36. Franklin, J. *et al.* Modeling plant species distributions under future climates: how fine scale do climate projections need to be? *Glob. Chang. Biol.* **19**, 473–483 (2013).

37. Lenoir, J. *et al.* Local temperatures inferred from plant communities suggest strong spatial buffering of climate warming across Northern Europe. *Glob. Chang. Biol.* **19**, 1470–1481 (2013).

38. Khaliq, I., Hof, C., Prinzinger, R., Bohning-Gaese, K. & Pfenninger, M. Global variation in thermal tolerances and vulnerability of endotherms to climate change. *Proc. R. Soc. B Biol. Sci.* **281**, 20141097–20141097 (2014).

39. Klein, T., Randin, C. & Körner, C. Water availability predicts forest canopy height at the global scale. *Ecol. Lett.* **18**, 1311–1320 (2015).

40. Meyer, C. *et al.* Range geometry and socio-economics dominate species-level biases in occurrence information. *Glob. Ecol. Biogeogr.* **25**, 1181–1193 (2016).

41. Oliver, R. Y., Meyer, C., Ranipeta, A., Winner, K. & Jetz, W. Global and national trends, gaps, and opportunities in documenting and monitoring species distributions. *PLOS Biol.* **19**, e3001336 (2021).

42. Zellweger, F. *et al.* Forest microclimate dynamics drive plant responses to warming. *Science.* **368**, 772–775 (2020).

43. Jackson, H. B. & Fahrig, L. Are ecologists conducting research at the optimal scale? *Glob. Ecol. Biogeogr.* **24**, 52–63 (2015).

44. Jetz, W., McPherson, J. M. & Guralnick, R. P. Integrating biodiversity distribution knowledge: toward a global map of life. *Trends Ecol. Evol.* **27**, 151–159 (2012).

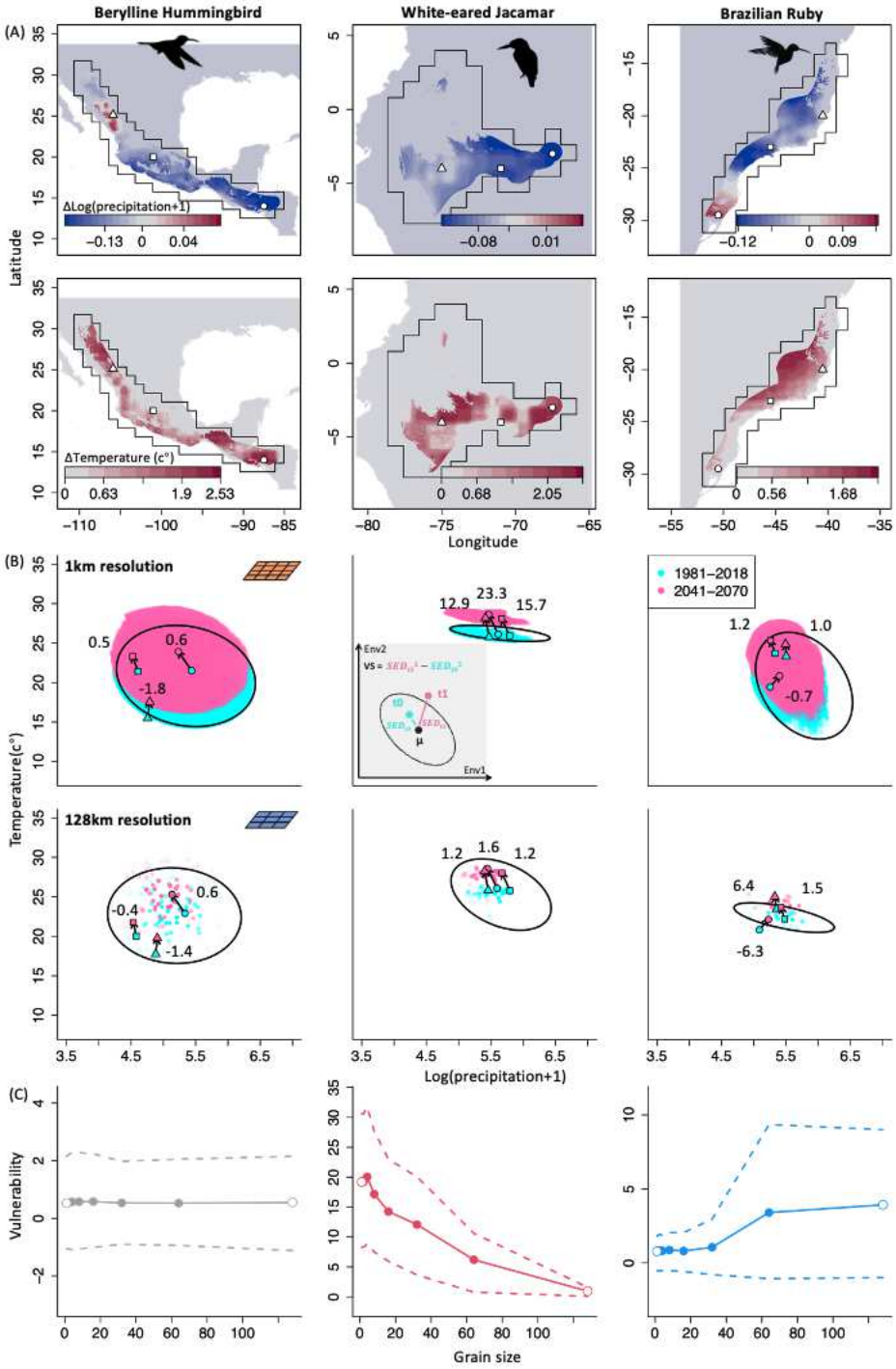

Figure 1. Scale-dependent climate change vulnerability in three New World bird species. (A) Projected change in temperature and precipitation between recent (1981-2018) and future (2041-2070) time periods, shown for 'local' grain size (1km; three example locations highlighted). Only pixels within the 80% quantile of the species' environmental niche are shown. The black contours show the outlines of the coarse-grain (128km) pixels covered by a

species' range map buffered by 100km. (B) Difference between recent (cyan points) and future (pink points) conditions shown in bivariate environment space and estimated from temporally annotated local- vs. coarse-grain occurrence data (1km vs. 128km grain). Black ellipses represent the 80% quantile of the species' realized environmental niches. These values serve as basis for calculating species-level vulnerability, as showcased for the three example locations highlighted in (A). The vulnerability score (VS) of each grain is calculated as the difference between the squared standardized Euclidean distances (SED) between recent and projected environmental conditions to the niche center, as demonstrated by the inset figure in the middle panel of (B). For details on the calculation of the vulnerability score, see figure 3. (C) Mean vulnerability within a species' buffered range weighted by grain-wise suitability plotted against grain size. Dashed lines show the 95% confidence intervals of the species-level vulnerability.

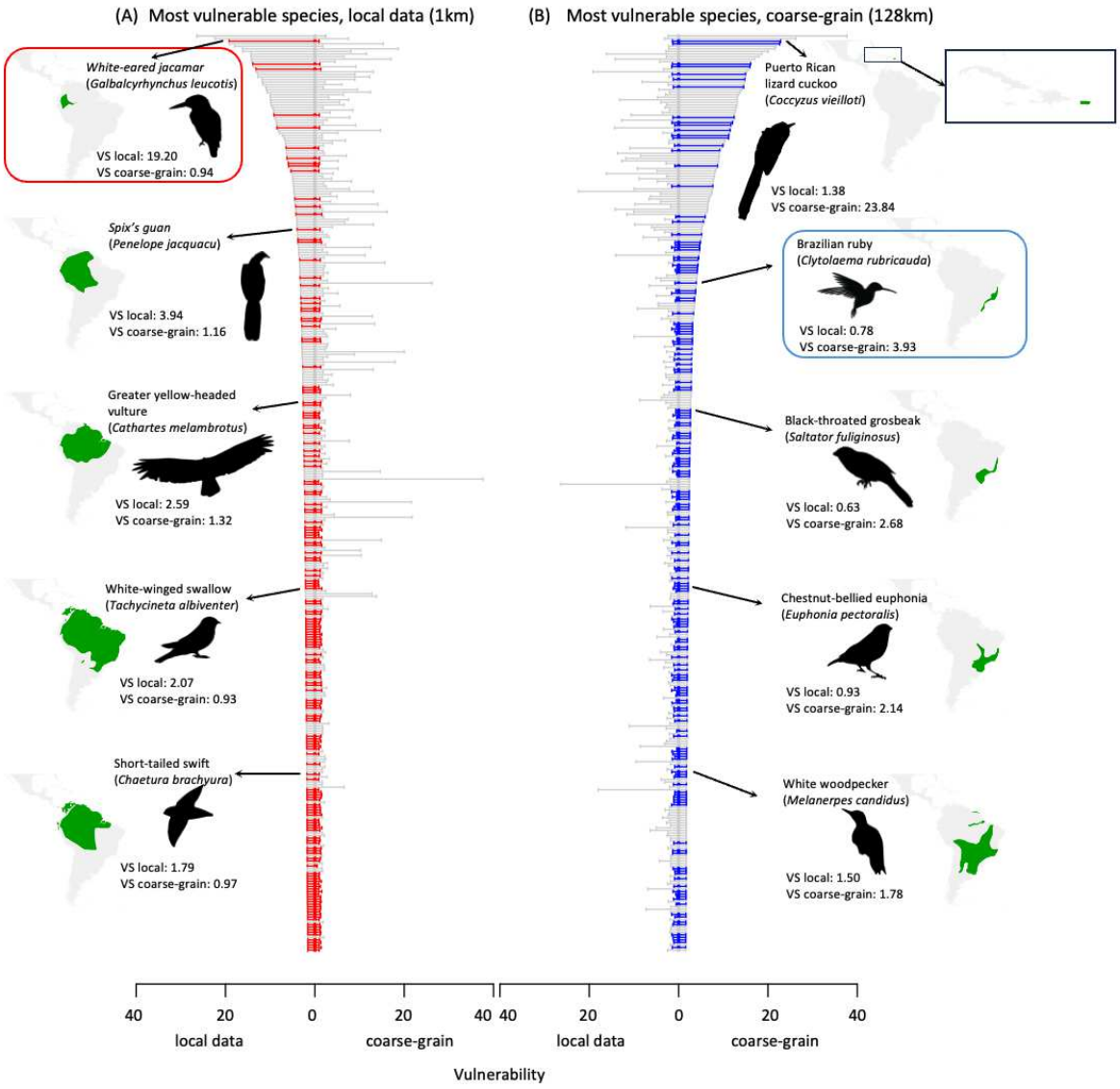

Figure 2. Discrepancy in species climate change vulnerability when assessed with local vs. coarse-grain data. 'VS' is short for 'Vulnerability score'. The graphs list the top 20% of species for each grain size, ranked by vulnerability. Red and blue colors identify species that are among the top 20% most vulnerable species for only one but not the other grain size, and grey the species that are shared between two grain sizes. Five example species per grain size are highlighted with their range maps (green) shown for spatial context. Colored frames show the two example species in Figure 1: the White-eared jacamar (*Galbalcyrhynchus leucotis*) and the Brazilian ruby (*Clytolaema rubricauda*).

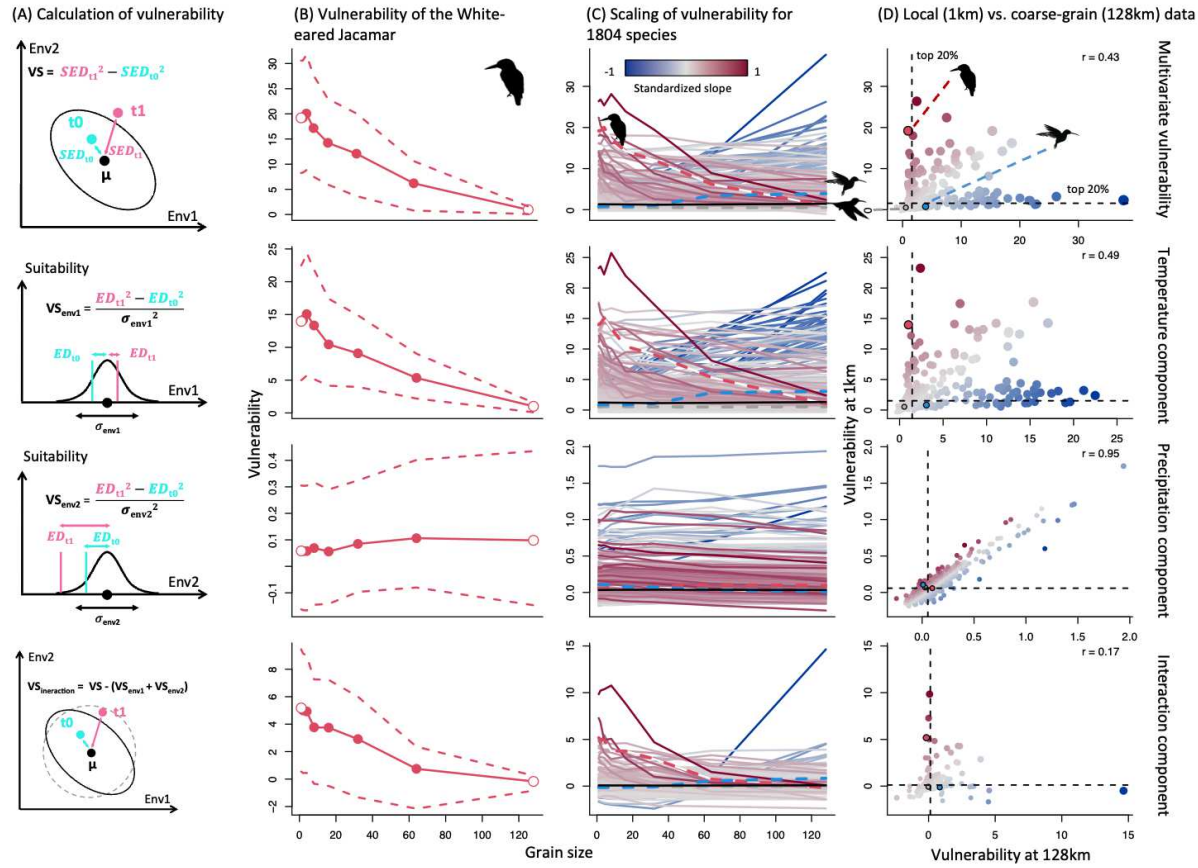

Figure 3. The scaling of vulnerability and its partitioned components. (A) The partitioning of the vulnerability of a site into univariate components and an interaction component. The inset in Figure 2 is shown in the first panel. μ represents the niche center, t_0 represents the recent environmental condition and t_1 represents the future environmental condition. The solid line ellipsoid represents the 95% quantile of the multivariate normal distribution of the realized niche. The dashed circle represents the 95% quantile of a multivariate normal distribution where there is no interaction between niche axes. The vulnerability score is calculated as the difference between the squared standardized Euclidean distances (SED) of the current and projected future environmental conditions to the niche center. In the one-dimensional case, it is the difference between the squared Euclidean distances (ED) divided by the one-dimensional niche breadth (the variance, σ^2). When there is no interaction among niche axes

(dashed circle), the multivariate vulnerability is just the sum of the univariate components. (B) Scaling of the multivariate vulnerability of the White-eared Jacamar and its partitioned components across its geographic range (weighted by pixel suitability). Dashed lines show the 95% confidence intervals of vulnerability. (C) Vulnerability scaling expanded to all 1804 assessed species. Colored lines represent individual species, with red indicating negative and blue positive vulnerability-scaling relationship and dashing marking the focal species shown in B). Black solid lines show the average across all species. (D) Comparison of vulnerability based on local vs. coarse-grain data 1804 species. Black dashed lines show the 80% quantiles of vulnerability at for each category, respectively.

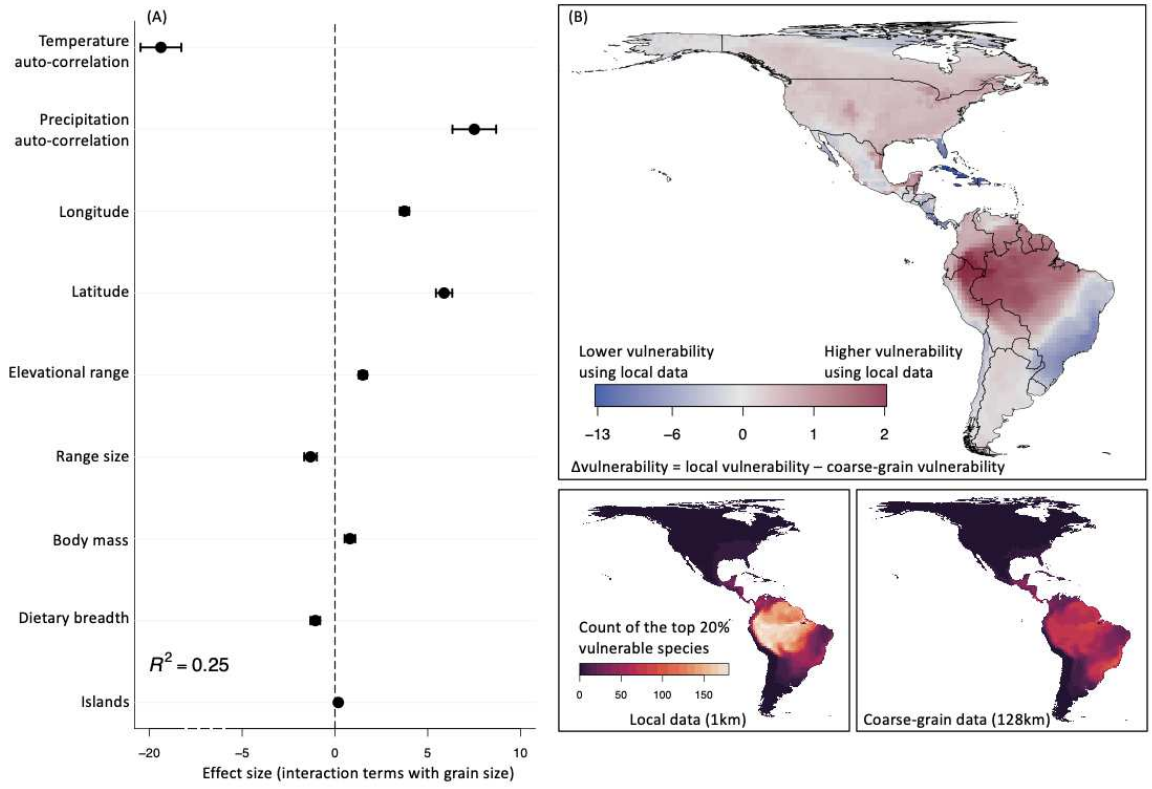

Figure 4. (A) The relative effects of nine hypothesized drivers on the spatial scaling of climate change vulnerability. Positive value means the larger the predictor is, the more likely the vulnerability is going to increase with grain size. Negative value means the larger the predictor is, the less likely the vulnerability is going to decrease with grain size. All nine predictors are combined in a single model. (B) Average difference (weighted by the inverse of range size) in species-level vulnerability of 128 km assemblages when assessed with local vs. coarse-grain data (local vulnerability minus coarse-grain vulnerability) based on1804 bird species (top panel). Negative values mean that coarse-grain data overestimate, positive values that coarse-grain data underestimate local vulnerability. Bottom panels show the count of the top 20% vulnerable species based on local (1km) vs. coarse-grain data (128km).

Methods

Occurrence Data

We obtained species' occurrence data from eBird[45]. We filtered eBird data to those that are observed within the breeding seasons (we use May to July as the approximate breeding season for the Northern Hemisphere; November to January for the Southern Hemisphere) between 1981 to 2018 (38 years) and within 1km traveling distance from the recorded coordinates. To reduce potential spatial biases, we further thinned occurrences to be at least 5km apart[46]. Results using 10km and 20km thinning distances are in the Extended Data (Extended Data Fig. 5-6). We only kept species with more than 20 occurrence records after thinning for further analysis, resulting in a final dataset of 1,804 species comprising 860,186 records representing the breeding seasons for these 38 years.

Environmental Data

We focused our niche assessment on temperature and precipitation, core climatic drivers of ecological processes[47,48] that were also the focus of prominent work addressing the biodiversity consequence of climate change[3,4,21]. We used CHELSA V2.1 data at 30'' (~1km) resolution[49,50] to derive a monthly timeseries for 1981 and 2018 and monthly averages for 2041 to 2070 based on two different CMIP6 models (GFDL-ESM4 and IPSL-CM6A-LR) and are used for SSP126, SSP370 and SSP585 scenarios. The results for GFDL-ESM4 SSP370 are shown in the main text, and the rest is provided in the Extended Data (Extended Data Fig. 7-9). We aggregated the environmental layers to 8 different resolutions on a log-2 scale (1, 2, 4, 8, 16, 32, 64 and 128km). The coarsest resolution corresponds roughly to the accuracy of species' expert range maps[22].

Species Attributes

To quantify range size, centroid latitude, centroid longitude, and spatial heterogeneity within its range, we for the same species used expert range maps from Jetz et al. (2012)[51] . We first buffered the range maps by 0.5 degree (~50km), and then calculated the proportion of occurrence points within the buffered range maps. If the proportion of points within the buffered range is less than 0.9, we first buffered the thinned occurrence data with 0.5 degree in both latitude and longitude and then merged them with the buffered range map to produce an updated range map; if the proportion of points is larger than 0.9, we used the original buffered range map. We then used the buffered range map to calculate species geographic range size, absolute centroid latitude, and longitude. We also used the map to calculate spatial heterogeneity characteristics of the landscape occupied by species using Moran's I within 10km distance for both the average temperature and average precipitation during the breeding seasons between 1981 to 2010. Moran's I is a coefficient of spatial autocorrelation, which we used as an inverse measure of spatial heterogeneity. Higher spatial autocorrelation represents lower spatial heterogeneity.

For 1759 of the 1804 total species we obtained data on mean and range of elevations occupied from Quintero and Jetz (2018)[52]. For the remainder, we derived this information from an overlay of their range map with a global elevation layer[53]. Dietary niche breadth and elevational range were used as proxies for habitat specialization. To account for the effect of island distribution, we calculated the proportion of occurrence points on (Caribbean) islands, and denote this variable as 'island'. We obtained species body mass and dietary data from the EltonTrait database[54]. Body mass was log transformed, and dietary breadth was calculated by Levin's niche breadth index[55], B.

$$B = 1/R \sum_i {p_i}^2$$

Where R is the number of dietary categories, p_i is the relative frequency of the corresponding dietary category.

Vulnerability measure

We developed a climate change vulnerability metric that incorporates sensitivity and exposure in the multivariate environmental space. Our metric allows additively partitioning a multivariate vulnerability score into its univariate components and an interaction component. A major advantage of this method is that beyond the consideration of magnitude of exposure, as provided by alternative popular measures[56–58]it also addresses the position and direction of exposure in the environmental space[59,60].

Consider a one-dimensional environmental space, denote $x_{i,t0}$ as the environmental condition of location i at the current time t_0, and $x_{i,t1}$ as the environmental condition of location i in the future time t_1. A simple climate change vulnerability score (VS) for the species at location i is the Euclidean distance (ED) between future and current climate, standardized by the species' realized niche breadth σ[61]:

$$VS_{i,naive} = \sqrt{\frac{(x_{i,t1}-x_{i,t0})^2}{\sigma^2}} \quad \dots (1)$$

Where the numerator $|x_{i,t1} - x_{i,t0}|$ measures the climate change exposure, and the denominator σ measures species' sensitivity to climate change. There are two major issues with this naïve metric: 1) by always assuming a positive number, it implies that climate change is always harmful to a species no matter the species' local suitability increases or decreases; 2) it assumes that exposure always has the same effect no matter the local population is in a favorable environment or unsuitable environment. A realistic vulnerability measure should 1) allow the local vulnerability to decrease if the condition becomes more favorable in the future; and 2) predict higher risk for populations that are already in unfavorable environments

given the same exposure because they are already stressed[62–64]. To achieve these goals, we propose a new vulnerability measure modified from equation 1:

$$VS_i = SED_{t1}^2 - SED_{t0}^2 = \frac{(x_{i,t1}-\mu)^2}{\sigma^2} - \frac{(x_{i,t0}-\mu)^2}{\sigma^2} \quad \ldots (2)$$

Where μ is the species' realized niche center. This metric quantifies the difference between two squared standardized Euclidean distances (SED): the SED between the current climatic condition at location *i* and species' niche center, and the SED between the future climatic condition at location *i* and species' niche center. By assuming that a species' niche center is most suitable for a population[65,66], this metric predicts that vulnerability will increase if climate change is moving the local population away from the niche center, and decrease if it is moving the local population towards the niche center. This metric also predicts higher risk for populations at the margin of the climatic niche. For example, raising the temperature by 1 σ, a population at the center of its niche will have a vulnerability score of $1^2 - 0^2 = 1$, while a population that's 2 σs away from the center will have a vulnerability score of $3^2 - 2^2 = 5$. When generalized to the n-dimensional climatic space, the standardized Euclidean distances in equation 2 are equivalent to the Mahalanobis distances[67], which are essentially standardized Euclidean distances calculated with principal components:

$$\begin{aligned} VS_i &= SED_{t1}^2 - SED_{t0}^2 \\ &= \left(x_{i,t1} - \mu\right)^T \Sigma^{-1} \left(x_{i,t1} - \mu\right) - \left(x_{i,t0} - \mu\right)^T \Sigma^{-1} \left(x_{i,t0} - \mu\right) \\ &= MD_{t1}^2 - MD_{t0}^2 = \Delta MD^2 \quad \ldots (3) \end{aligned}$$

Where $x_{i,t1}$, $x_{i,t0}$ and μ vectors of environmental variables with length n, and Σ is an n by n covariance matrix estimated from species' realized niche. Using a novel partitioning framework, the Mahalanobis distances can be written as the sum of univariate SED and an interaction component. The interaction component measures how much the correlations among niche axes decrease or increase the standardized Euclidean distance between an

environmental condition and the niche center[68]. Take a two-dimensional climatic space for example, and let x and y be the two climatic variables, the squared Mahalanobis distance between the local climate and species' niche center is:

$$MD^2 = \frac{{d_x}^2}{\sigma_x^2} + \frac{{d_y}^2}{\sigma_y^2} + \frac{1}{|\Sigma|}\left(\rho^2\left(d_x\sigma_x - d_y\sigma_y\right)^2 + 2\rho d_x d_y \sigma_x \sigma_y(\rho - 1)\right)$$

$$= MD_x^2 + MD_y^2 + MD_{interaction}^2 \ldots (4)$$

Where $d_x = x - \mu$, $d_y = y - \mu$, ρ is the correlation between x and y in the covariance matrix Σ, and $|\Sigma|$ is the determinant of the covariance matrix. Subsisting equation 4 into equation 3, the climate change vulnerability for a two-dimensional climatic space is:

$$VS_i = MD_{t1}^2 - MD_{t0}^2 = \Delta MD^2$$

$$= VS_x + VS_y + VS_{interaction}$$

$$= \frac{{d_{x,t1}}^2}{\sigma_x^2} - \frac{{d_{x,t0}}^2}{\sigma_x^2} + \frac{{d_{y,t1}}^2}{\sigma_y^2} - \frac{{d_{y,t0}}^2}{\sigma_y^2}$$

$$+ \frac{1}{|\Sigma|}\left(\rho^2\left(d_{x,t1}\sigma_x - d_{y,t1}\sigma_y\right)^2 + 2\rho d_{x,t1} d_{y,t1} \sigma_x \sigma_y(\rho - 1)\right)$$

$$- \frac{1}{|\Sigma|}\left(\rho^2\left(d_{x,t0}\sigma_x - d_{y,t0}\sigma_y\right)^2 + 2\rho d_{x,t0} d_{y,t0} \sigma_x \sigma_y(\rho - 1)\right)$$

… (5)

Which partitions multivariate vulnerability into univariate components and an interaction component, therefore allowing us to compare their relative importance (Fig. 3A).

The species-level climate change vulnerability was calculated by averaging the local vulnerability across the grains within a species' range. However, because of the high false presence rate within the range maps at finer grains[22], the unsuitable locations will be overly represented by equation 4. To account for this false presence, we weighed the vulnerability of each location *i* by its climatic suitability:

$$E(VS) = \sum_i^k \frac{w_i}{\sum w_i} VS_i \quad \ldots (6)$$

In this paper, we used the suitability at time *t*0 derived from the kernel of a Gaussian distribution [69] as weights:

$$w_i = e^{-(x_{i,t0}-\mu)^T \Sigma^{-1} (x_{i,t0}-\mu)} \ldots (7)$$

This suitability ranges from 0 to 1, with 1 representing the suitability at the species' niche center (assumed to be the optimal condition).

This procedure effectively controls for the effect of false presence because sites with false presence probability are likely to occupy less suitable climatic conditions. They will be assigned with low suitability scores and therefore lower weights in the species-level vulnerability score. Biologically, because the normalized suitability score represents the relative occurrence rate of a species at a site[70], equation 6 can be interpreted as the expected vulnerability across a species' geographic range.

Because the Mahalanobis distance follows a chi-square distribution in which the degrees of freedom equal to the total number of dimensions[69], our vulnerability score (VS) also has a probabilistic interpretation: when the dimension is two, an increase of VS from 0 to 0.45 is equivalent to a 20% drop of suitability relative to the suitability estimated at a species' niche center; an increase of VS from 0 to 1 is equivalent to a 40% drop of suitability and an increase of VS from 0 to 2 is equivalent to a 63% drop of suitability.

Statistical analysis

For each species, we extracted for each occurrence record the mean temperature and precipitation during the breeding seasons of the recorded year (this accounts for annual temporal variation in climatic conditions). A species' environmental niche center μ, and the covariance matrix Σ were estimated by the average of 100 random samples of occurrence points spatial thinned by 'spThin'. We then calculated the climate change vulnerability using

the 30-years average temperature and precipitation between 1981 and 2018 as x_{t0}, and the projected average climate between 2041 and 2070 as x_{t1} (equation 3-5). Species-level vulnerability was calculated as the average pixel-level vulnerability within the buffered range weighted by pixel-level suitability (equation 6-7). We calculated the species-level vulnerability for all 1,804 species at eight grain sizes. We used correlation plots to demonstrate the pairwise comparison between species-level vulnerability calculated at different grain sizes.

We used linear mixed effect model to examine the scale-dependence of species-level vulnerability[71]. The species-level weighted mean vulnerability across a species' geographical range was the response variable. We modeled grain size, range size, temperature autocorrelation, precipitation autocorrelation, elevational range, mean elevation, body mass, dietary niche breadth, proportion of points on islands, centroid latitude, and longitude, and the interaction terms between grain size and all previously mentioned predictors as fixed effects. Species identity was included as a random effect on the intercept.

To show the spatial pattern of the scale-dependence of species-level climate change vulnerability, we mapped the mean scale-dependence for species distributed within each 128km grid cell, weighted by the inverse of range size to control for the effect of wide-ranged species. The scale-dependence for each species was calculated as the difference between vulnerability calculated at the 1km grain and 128km grain. Positive value means that the fine grain vulnerability estimate is larger than the coarse grain vulnerability estimation; negative value means the opposite. We also mapped the number of the most vulnerable species (defined as the 20% most vulnerable species) quantified at 1km grain and 128km grain. Behrmann equal-area projection was used for mapping.

Data availability

All datasets used here are publicly available. The occurrence data are available from eBird website https://science.ebird.org/en/use-ebird-data. The climatic data are available from CHELSA website https://chelsa-climate.org. Trait datasets are available from https://figshare.com/collections/EltonTraits_1_0_Species-level_foraging_attributes_of_the_world_s_birds_and_mammals/3306933.

Code availability

Computer code used in the analysis is available on request from the corresponding author.

Acknowledgements

We thank Jetz lab members for discussion and comments on the manuscript.

Author contributions

M.L. and W.J. conceived the study. M.L. processed the data and performed the analysis. M.L. and W.J. wrote the manuscript.

45. Sullivan, B. L. *et al.* eBird: A citizen-based bird observation network in the biological sciences. *Biol. Conserv.* **142**, 2282–2292 (2009).

46. Aiello-Lammens, M. E., Boria, R. A., Radosavljevic, A., Vilela, B. & Anderson, R. P. spThin: An R package for spatial thinning of species occurrence records for use in ecological niche models. *Ecography.* **38**, 541–545 (2015).

47. Jetz, W. & Rahbek, C. Geographic range size and determinants of avian species richness. *Science.* **297**, 1548–1551 (2002).

48. Kreft, H. & Jetz, W. Global patterns and determinants of vascular plant diversity. *Proc. Natl. Acad. Sci.* **104**, 5925–5930 (2007).

49. Karger, D. N. *et al.* Climatologies at high resolution for the earth's land surface areas. *Sci. Data* **4**, 1–20 (2017).

50. Karger, D. N., Wilson, A. M., Mahony, C., Zimmermann, N. E. & Jetz, W. Global daily 1 km land surface precipitation based on cloud cover-informed downscaling. *Sci. Data* **8**, 307 (2021).

51. Jetz, W., Thomas, G. H., Joy, J. B., Hartmann, K. & Mooers, a O. The global diversity of birds in space and time. *Nature* **491**, 444–448 (2012).

52. Quintero, I. & Jetz, W. Global elevational diversity and diversification of birds. *Nature* **555**, 246–250 (2018).

53. Amatulli, G. *et al.* A suite of global, cross-scale topographic variables for environmental and biodiversity modeling. *Sci. Data* **5**, 180040 (2018).

54. Wilman, H. *et al.* EltonTraits 1.0: Species-level foraging attributes of the world's birds and mammals. *Ecology* **95**, 2027–2027 (2014).

55. Feinsinger, P., Spears, E. E. & Poole, R. W. A simple measure of niche breadth. *Ecology* **62**, 27–32 (1981).

56. Rinnan, D. S. & Lawler, J. Climate-niche factor analysis: A spatial approach to quantifying species vulnerability to climate change. *Ecography.* **42**, 1494–1503 (2019).

57. Dickinson, M. G., Orme, C. D. L., Suttle, K. B. & Mace, G. M. Separating sensitivity from exposure in assessing extinction risk from climate change. *Sci. Rep.* **4**, 6898 (2015).

58. Williams, J. W., Jackson, S. T. & Kutzbach, J. E. Projected distributions of novel and disappearing climates by 2100 AD. *Proc. Natl. Acad. Sci.* **104**, 5738–5742 (2007).

59. Mahony, C. R. & Cannon, A. J. Wetter summers can intensify departures from natural variability in a warming climate. *Nat. Commun.* **9**, 783 (2018).

60. Kling, M. M., Auer, S. L., Comer, P. J., Ackerly, D. D. & Hamilton, H. Multiple axes of ecological vulnerability to climate change. *Glob. Chang. Biol.* **26**, 2798–2813 (2020).

61. Williams, J. W., Jackson, S. T. & Kutzbach, J. E. Projected distributions of novel and disappearing climates by 2100 AD. *Proc. Natl. Acad. Sci.* **104**, 5738–5742 (2007).

62. Abeli, T., Gentili, R., Mondoni, A., Orsenigo, S. & Rossi, G. Effects of marginality on plant population performance. *J. Biogeogr.* **41**, 239–249 (2014).

63. Sexton, J. P., McIntyre, P. J., Angert, A. L. & Rice, K. J. Evolution and ecology of species range limits. *Annu. Rev. Ecol. Evol. Syst.* **40**, 415–436 (2009).

64. Margalef-Marrase, J., Pérez-Navarro, M. Á. & Lloret, F. Relationship between heatwave-induced forest die-off and climatic suitability in multiple tree species. *Glob. Chang. Biol.* **26**, 3134–3146 (2020).

65. Osorio-Olvera, L., Yañez-Arenas, C., Martínez-Meyer, E. & Peterson, A. T. Relationships between population densities and niche-centroid distances in North American birds. *Ecol. Lett.* **23**, 555–564 (2020).

66. de la Fuente, A., Hirsch, B. T., Cernusak, L. A. & Williams, S. E. Predicting species abundance by implementing the ecological niche theory. *Ecography.* **44**, 1723–1730 (2021).

67. Mahony, C. R., Cannon, A. J., Wang, T. & Aitken, S. N. A closer look at novel climates: New methods and insights at continental to landscape scales. *Glob. Chang. Biol.* **23**, 3934–3955 (2017).

68. Lu, M., Winner, K. & Jetz, W. A unifying framework for quantifying and comparing n-dimensional hypervolumes. *Methods Ecol. Evol.* **12**, 1953–1968 (2021).

69. Etherington, T. R. Mahalanobis distances and ecological niche modelling: Correcting a chi-squared probability error. *PeerJ* **2019**, 1–8 (2019).

70. Merow, C., Smith, M. J. & Silander, J. A. A practical guide to MaxEnt for modeling species' distributions: What it does, and why inputs and settings matter. *Ecography.* **36**, 1058–1069 (2013).

71. Bates, D., Mächler, M., Bolker, B. & Walker, S. Fitting linear mixed-effects models using lme4. *J. Stat. Softw.* **67**, (2015).

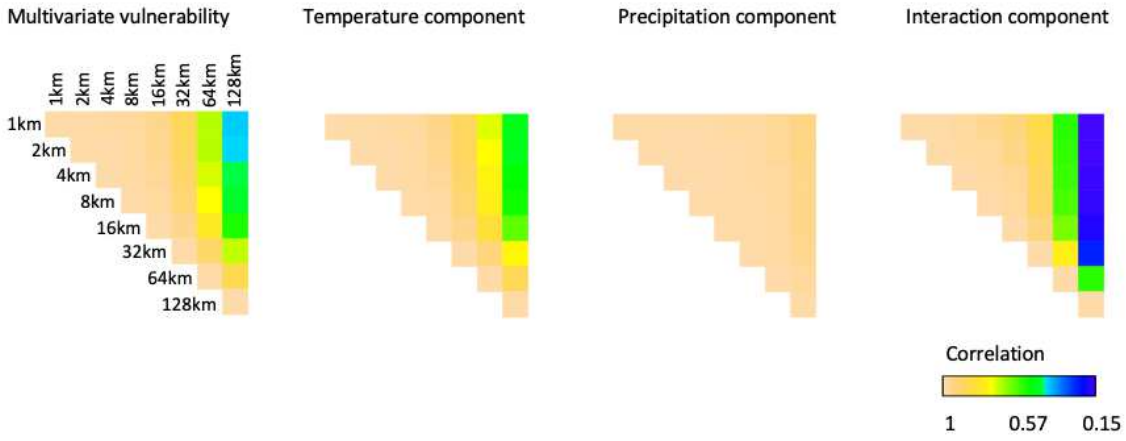

Extended Data Figure 1. Pairwise correlation between vulnerability score calculated at different grain size for the 1809 species. The multivariate vulnerability score equals the sum of the three partitioned components.

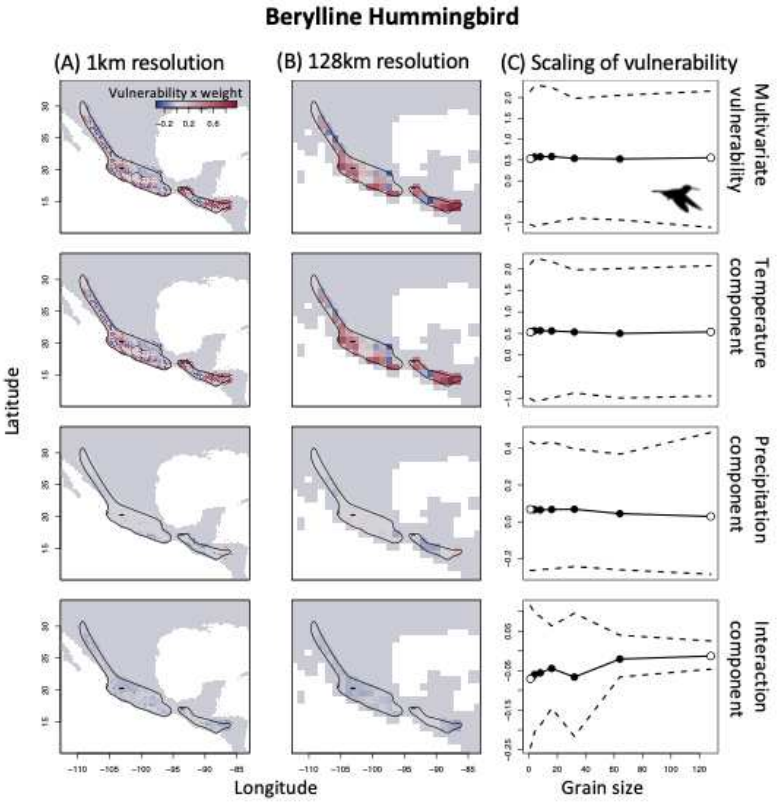

Extended Data Figure 2. (A) Maps of vulnerability multiplied by suitability at the 1km resolution for the Berylline hummingbird (*Amazilia beryllina*). (B) Maps of vulnerability multiplied by suitability at the 128km resolution. (C) Mean multivariate vulnerability as well as the partitioned components within a species' range weighted by suitability plotted against grain size. Dashed lines show the 95% confidence intervals of weighted vulnerability.

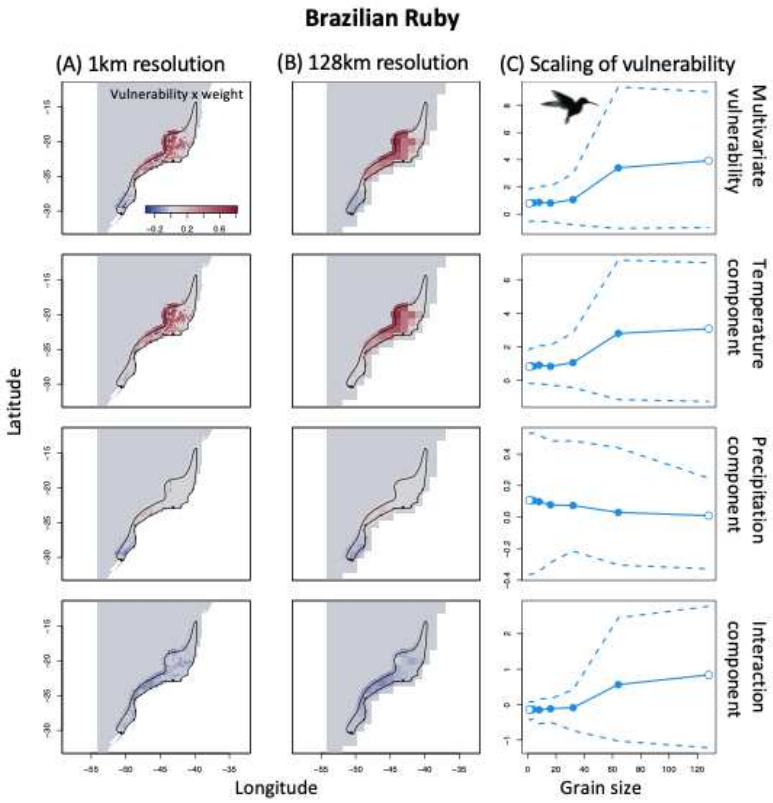

Extended Data Figure 3. (A) Maps of vulnerability multiplied by suitability at the 1km resolution for the Brazilian Ruby (*Clytolaema rubricauda*). (B) Maps of vulnerability multiplied by suitability at the 128km resolution. (C) Mean multivariate vulnerability as well as the partitioned components within a species' range weighted by suitability plotted against grain size. Dashed lines show the 95% confidence intervals of weighted vulnerability.

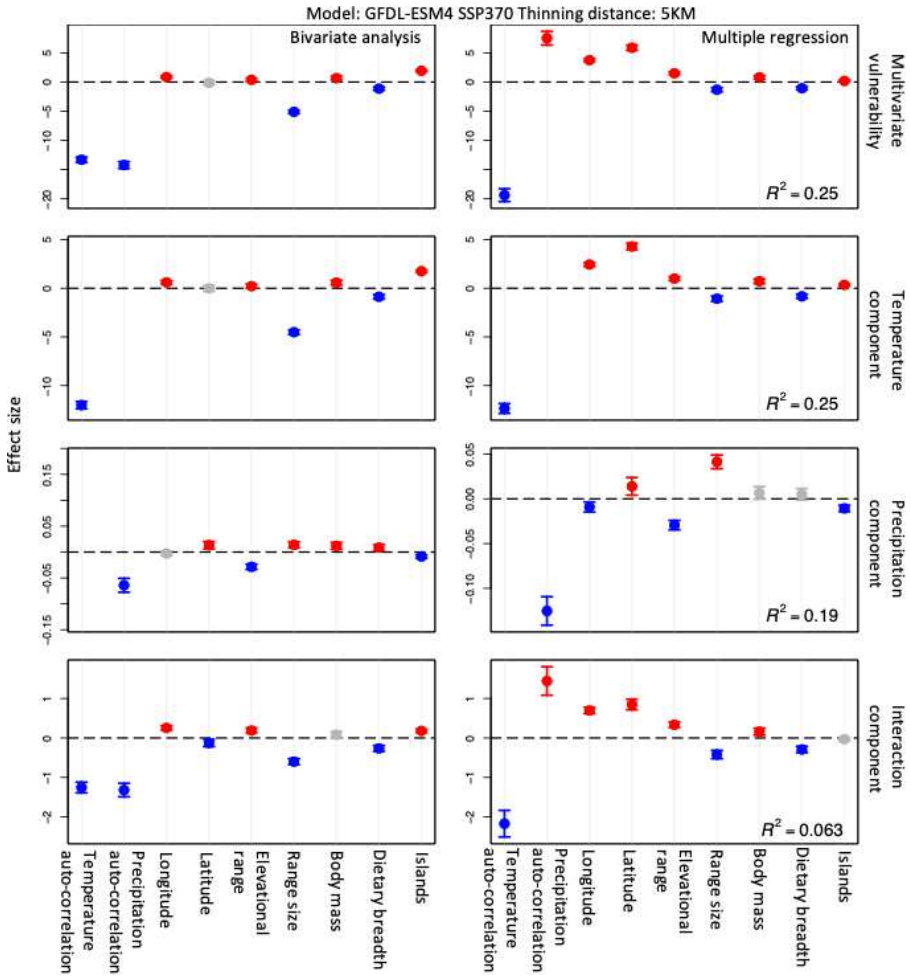

Extended Data Figure 4. Effect size of predictors on the slope of vulnerability-scale relationships (interaction terms between predictor and grain size) using linear mixed effect models. The projection model is GFDL-ESM4 SSP370. 5km spatial thinning is used. There are in total 1804 species in the analysis. The first row shows models using the multivariate vulnerability as the response variable. The second to the fourth row shows models using the partitioned components as response variables. Species' ID is modeled as a random effect on the intercept. x-axis shows the predicting variables. The left column shows the results of the bivariate analysis (vulnerability as response, grain size, one covariate, and their interaction term as predictors). The right column shows the results of the multivariate analysis.

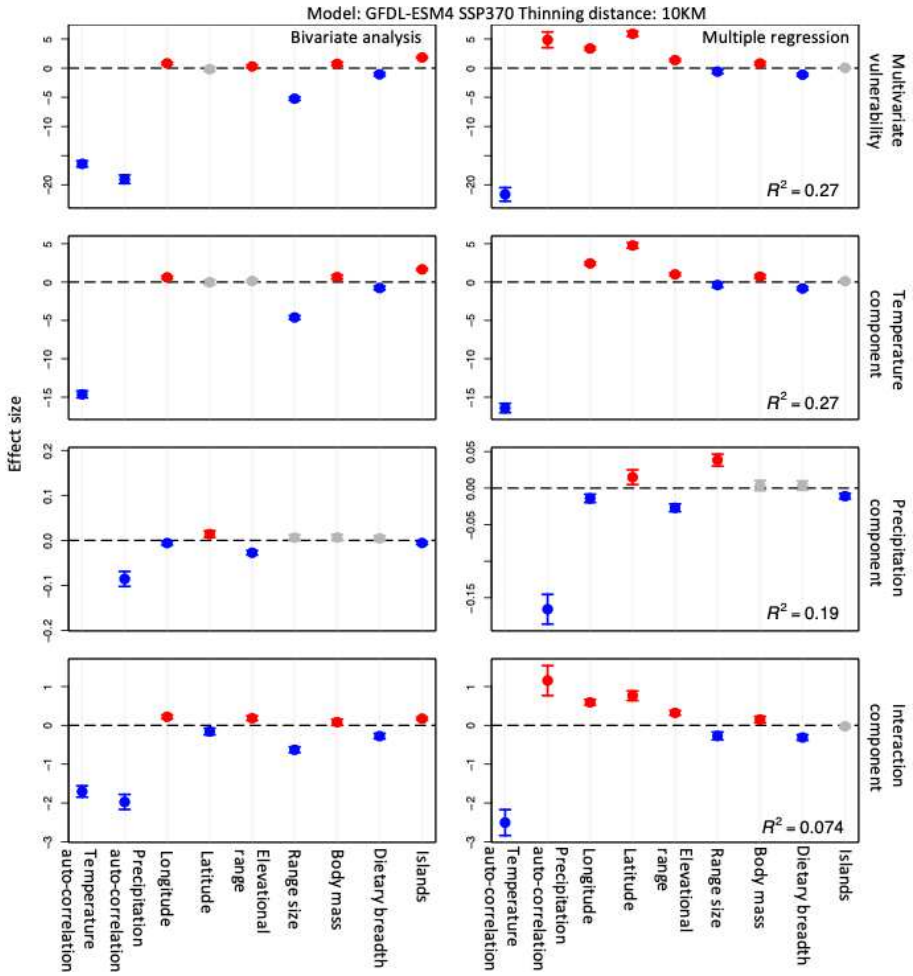

Extended Data Figure 5. Effect size of predictors on the slope of vulnerability-scale relationships (interaction terms between predictor and grain size) using linear mixed effect models. The projection model is GFDL-ESM4 SSP370. 10km spatial thinning is used. There are in total 1703 species in the analysis. The first row shows models using the multivariate vulnerability as the response variable. The second to the fourth row shows models using the partitioned components as response variables. Species' ID is modeled as a random effect on the intercept. x-axis shows the predicting variables. The left column shows the results of the bivariate analysis (vulnerability as response, grain size, one covariate, and their interaction term as predictors). The right column shows the results of the multivariate analysis.

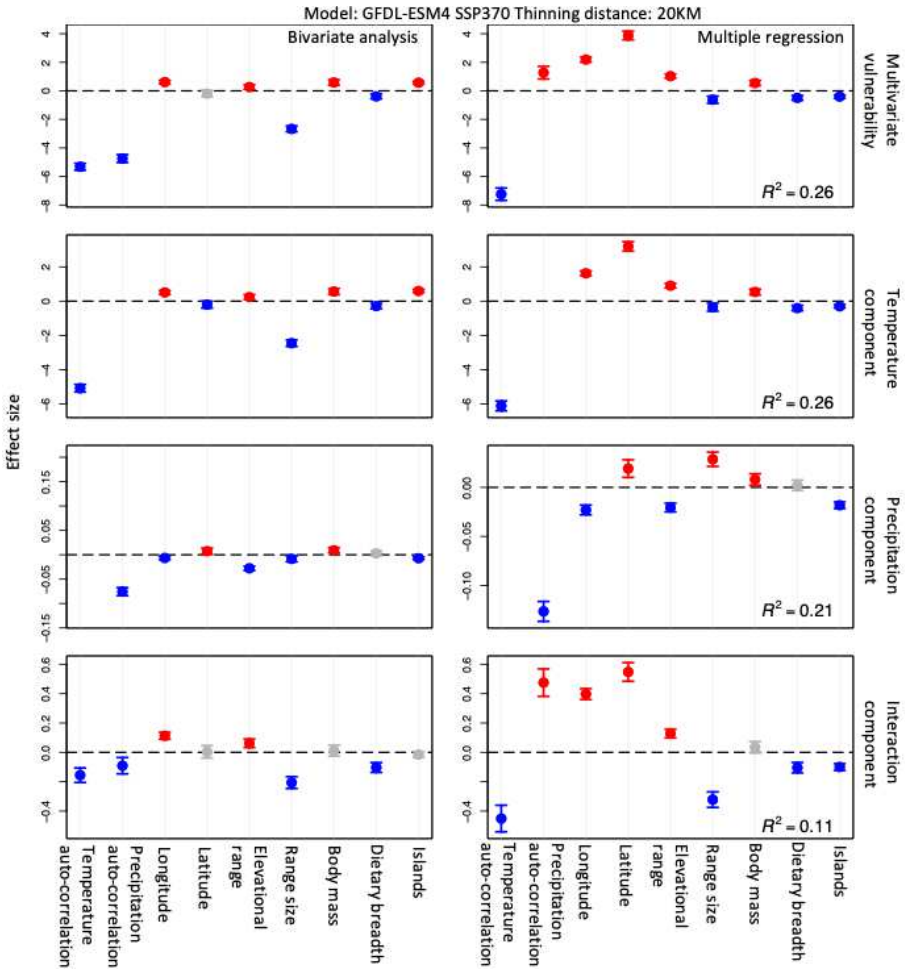

Extended Data Figure 6. Effect size of predictors on the slope of vulnerability-scale relationships (interaction terms between predictor and grain size) using linear mixed effect models. The projection model is GFDL-ESM4 SSP370. 20km spatial thinning is used. There are in total 1546 species in the analysis. The first row shows models using the multivariate vulnerability as the response variable. The second to the fourth row shows models using the partitioned components as response variables. Species' ID is modeled as a random effect on the intercept. x-axis shows the predicting variables. The left column shows the results of the bivariate analysis (vulnerability as response, grain size, one covariate, and their interaction term as predictors). The right column shows the results of the multivariate analysis.

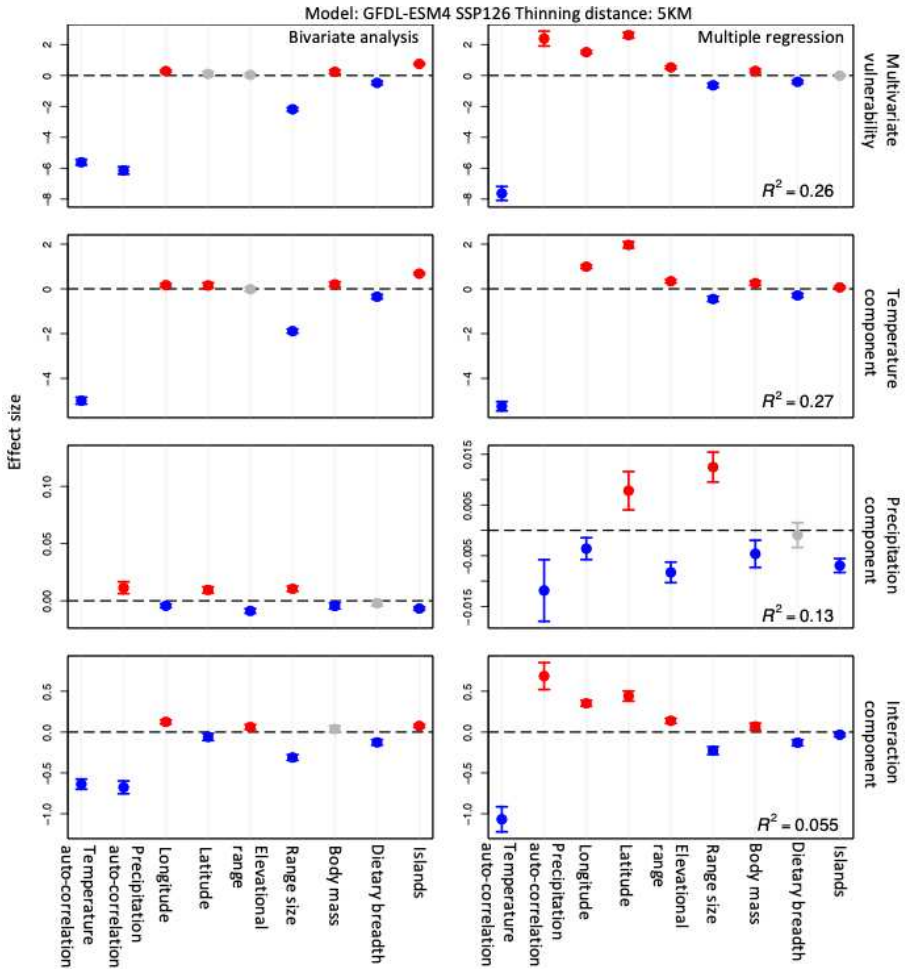

Extended Data Figure 7. Effect size of predictors on the slope of vulnerability-scale relationships (interaction terms between predictor and grain size) using linear mixed effect models. The projection model is GFDL-ESM4 SSP126. 5km spatial thinning is used. There are in total 1804 species in the analysis. The first row shows models using the multivariate vulnerability as the response variable. The second to the fourth row shows models using the partitioned components as response variables. Species' ID is modeled as a random effect on the intercept. x-axis shows the predicting variables. The left column shows the results of the bivariate analysis (vulnerability as response, grain size, one covariate, and their interaction term as predictors). The right column shows the results of the multivariate analysis.

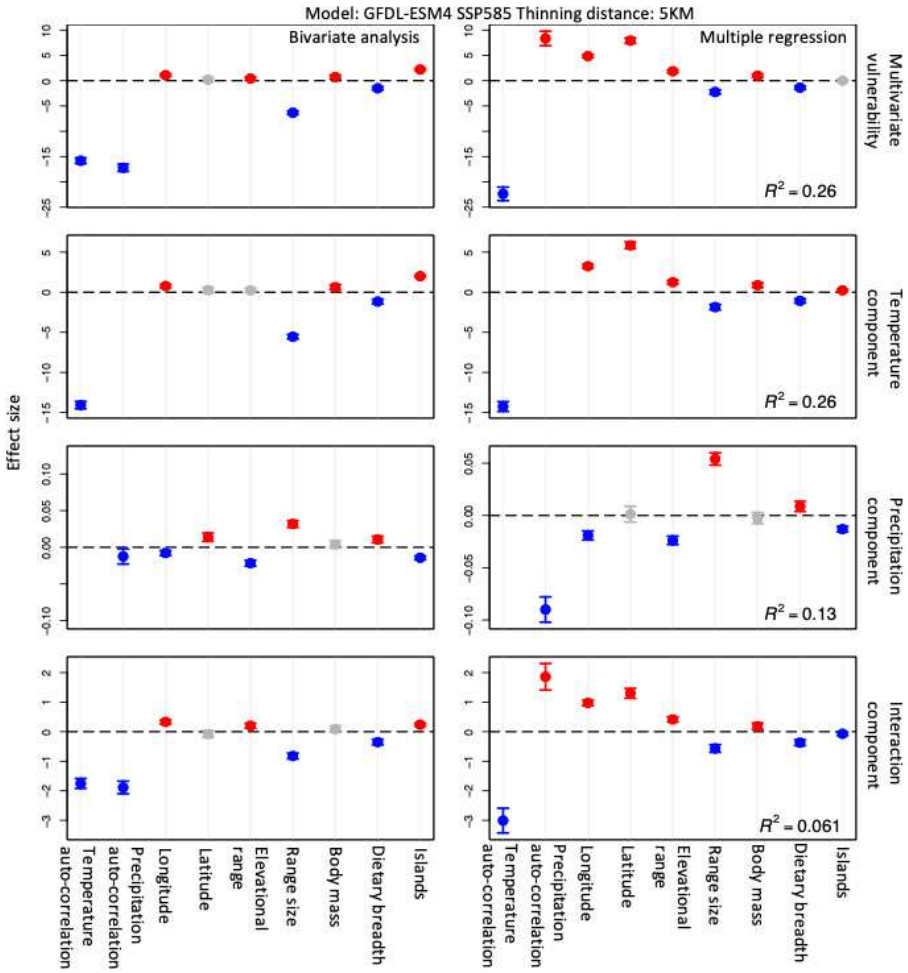

Extended Data Figure 8. Effect size of predictors on the slope of vulnerability-scale relationships (interaction terms between predictor and grain size) using linear mixed effect models. The projection model is GFDL-ESM4 SSP585. 5km spatial thinning is used. There are in total 1804 species in the analysis. The first row shows models using the multivariate vulnerability as the response variable. The second to the fourth row shows models using the partitioned components as response variables. Species' ID is modeled as a random effect on the intercept. x-axis shows the predicting variables. The left column shows the results of the bivariate analysis (vulnerability as response, grain size, one covariate, and their interaction term as predictors). The right column shows the results of the multivariate analysis.

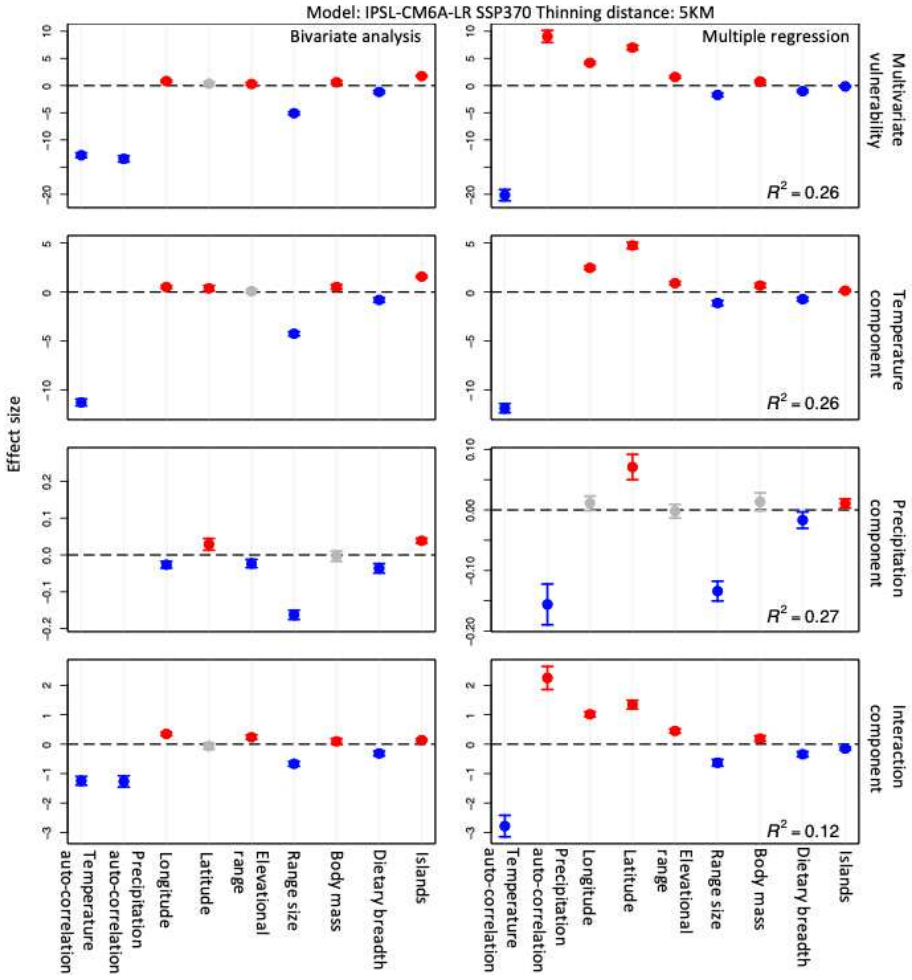

Extended Data Figure 9. Effect size of predictors on the slope of vulnerability-scale relationships (interaction terms between predictor and grain size) using linear mixed effect models. The projection model is ISPL-CM6A-LR SSP370. 5km spatial thinning is used. There are in total 1804 species in the analysis. The first row shows models using the multivariate vulnerability as the response variable. The second to the fourth row shows models using the partitioned components as response variables. Species' ID is modeled as a random effect on the intercept. x-axis shows the predicting variables. The left column shows the results of the bivariate analysis (vulnerability as response, grain size, one covariate, and their interaction term as predictors). The right column shows the results of the multivariate analysis.

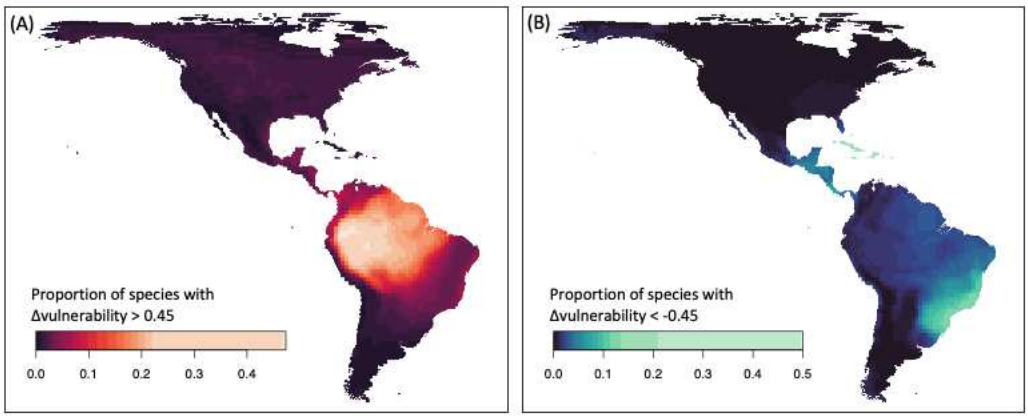

Extended Data Figure 10. (A) Proportion of species with Δvulnerability (local vulnerability minus coarse-grain vulnerability) > 0.45 in the local 128 km grid cells. (B) Proportion of species with Δvulnerability < -0.45 in the local 128 km grid cells.